Composites Science and Technology 234 (2023) 109924

Contents lists available at ScienceDirect

Composites Science and Technology

journal homepage: www.elsevier.com/locate/compscitech

# Development of pseudo-ductile interlayer hybrid composites of standard thickness plies by interleaving polyamide 6 nanofibrous layers

Salvatore Giacomo Marino [a], Eva Kuželová Košťáková [b], Gergely Czél [a,*]

[a] Department of Polymer Engineering, Faculty of Mechanical Engineering, Budapest University of Technology and Economics, Műegyetem rkp. 3, H-1111, Budapest, Hungary

[b] Department of Chemistry, Faculty of Science, Humanities and Education, Technical University of Liberec, Studentská 2, 461 17, Liberec, Czech Republic

ARTICLE INFO

Handling Editor: Marino Quaresimin

*Keywords:*
A. Hybrid composites
A. Layered structures
B. Fragmentation
Pseudo-ductility

ABSTRACT

A practical and effective way to provide fibre reinforced polymer composites with a safety margin before the final failure and a stable damage process is explored in this study. Mode II interlaminar fracture toughness has been increased in the hybrid composites made with standard thickness carbon/glass-epoxy plies by interleaving polyamide 6 nanofibrous layers between the carbon/epoxy and the glass/epoxy layers. The hybrid laminates exhibited pseudo-ductile behaviour, based on the fragmentation of the carbon/epoxy layer. The simple manufacturing method, by treating nanofibrous layers as "veils" to be stacked between prepregs sheets, revealed potential for large-scale application of this technique. Further enhancement of the material's mode II fracture toughness has been demonstrated by stacking multiple nanofibrous layers together.

## 1. Introduction

Unstable damage modes in fibre reinforced polymer composites (FRPC), frequently characterised by the sudden spread of delamination, strongly limit the potential of composite materials, which have excellent mechanical properties and low density. The development of delamination resistant composites is essential for making composites safer and more suitable for high-performance applications, e.g. aerospace industry. Several practical solutions for improving the toughness in composites, which is the material's ability to resist crack propagation, are proposed in the literature and some concern the introduction of toughening interlayers in the laminates [1–6].

The recently developed hybrid composites [7], particularly pseudo-ductile composites [8,9], have shown the possibility of mimicking the ductile behaviour typical of metals exhibited by a stable, progressive yielding phase in their non-linear stress-strain response under tensile loads. This non-linear part may be considered as a safety margin before the final failure of the material. Czél et al. [8] demonstrated that the parameters enabling pseudo-ductility in continuous, unidirectional (UD) interlayer hybrid composites under tensile loads are i) a significant difference between the stiffnesses of the constituent layers as well as their failure strains, and ii) the high mode II interlaminar fracture toughness ($G_{IIC}$) which is needed to suppress delamination.

We recently explored in Refs. [10,11] the possibility of promoting stable damage mechanisms through interleaving thermoset or thermoplastic films in carbon/glass-epoxy hybrid composites, achieving pseudo-ductility by fine-tuning the local fibre volume fraction at the layer interfaces and reducing the strain energy release rate at the fracture of the carbon/epoxy layer. In turn, the extra film interleaves slightly increased the hybrid materials' thickness, resulting in reduced overall elastic modulus and strength.

Promising results in terms of added toughness are presented by interleaving nanofibrous layers in monolithic (i.e. non-hybrid) composites [2,4,5,12–19]. The presence of the nanofibres enables favourable toughening mechanisms such as crack deviating or arresting mechanisms, which can increase the fracture toughness of the interleaved laminates. The toughening effect is commonly attributed to the bridging of the delamination crack by nanofibres and the energy dissipated by their yielding. These mechanisms are dominant in Mode I propagation of the delamination crack (i.e. opening). In mode II (i.e. shearing), the nanofibres can promote crack deviating and bifurcating mechanisms. The influence of nanofibres was studied in carbon/glass hybrid composites [14], measuring a toughness intermediate between the values found for the relevant non-hybrid laminates (i.e. carbon-only or glass-only laminates). Furthermore, thin nanofibrous

* Corresponding author.
*E-mail addresses:* marinos@pt.bme.hu (S.G. Marino), eva.kostakova@tul.cz (E.K. Košťáková), czel@pt.bme.hu (G. Czél).

https://doi.org/10.1016/j.compscitech.2023.109924
Received 21 June 2022; Received in revised form 14 November 2022; Accepted 13 January 2023
Available online 14 January 2023

mats have a minimal impact on the thickness and weight of the interleaved composites [4], making them more attractive than thermoplastic or thermoset films. Commonly, nanofibres are electrospun directly on the reinforcing fibres and impregnated with the resin together with them, i.e. with resin infusion technique. The possibility of having self-standing, flexible nanofibrous layers, e.g. available in a thin "veil" format, would make the stacking process with fibre reinforced prepregs easier to perform, and it would allow for the possibility of combining multiple nanofibrous layers to achieve higher areal densities.

## 2. Concept and design

The main objective of this study is to enable pseudo-ductility in originally unstable hybrid composite laminates, made by low cost, standard thickness, unidirectional (UD) carbon/epoxy (CF/EP) and S-glass/epoxy (GF/EP) plies, by introducing nanofibrous layers (NL) to the CF/EP and GF/EP interfaces for i) suppressing the delamination expected after the first crack of the CF/EP layer, and ii) promoting further CF/EP fragmentation to generate a stable pseudo-ductile failure process. A schematic representation of the proposed laminate architecture is presented in Fig. 1. The hybrid materials are prepared as a sandwich-type layup, made by a CF/EP layer between two glass/epoxy layers.

The laminates' design was made using the damage mode map, which is a tool developed for predicting damage modes in hybrid laminates in the function of the thickness of the fibre-reinforced layers [20,21]. Carbon/glass-epoxy hybrid laminates exhibit a multi-stage stress-strain response that may be unstable (i.e. characterised by catastrophic delamination after the first crack of the CF/EP layer) or stable (i.e. pseudo-ductile behaviour based on the fragmentation of the CF/EP layer and stable delamination around the fractures). The hybrid laminates were here designed for i) avoiding the failure of the glass/epoxy (GF/EP) layers together with the first fracture of the CF/EP layer; ii) promoting stable damage modes (i.e. fragmentation, stable delamination) and iii) maximising the thicknesses ratio of the CF/EP and GF/EP layers to increase the initial elastic modulus of the hybrid laminates significantly. The third requirement is a key aspect of this study, considering that pseudo-ductile glass-carbon hybrid composites in the past were mostly designed using special and expensive thin CF/EP plies [7,8], which released low energy at their first fracture due to their low thickness and therefore were not prone to delamination. In this study, we are demonstrating pseudo-ductility in hybrid composites made with cheaper standard thickness high strength CF/EP plies.

The mechanical behaviour of the baseline configuration (Fig. 1 (a)) under tensile loads was analysed in Ref. [10]. The baseline samples have the layup sequence [$G_3$/C/$G_3$], where [G] and [C] stand for GF/EP and CF/EP plies in the layup sequence, respectively; subscripts refer to the number of plies forming the layer. Although the configuration [$G_3$/C/$G_3$] had an unstable damage mode dominated by catastrophic delamination after the first fracture of the CF/EP layer, we expect to enable the fragmentation of the CF/EP layer by inserting polyamide 6 (PA6) nanofibrous layers that can increase the interlaminar fracture toughness [4,13,22] and suppress delamination.

Special specimens with a cut in the CF/EP layer across the fibres (see Fig. 1) were also made to study the mode II fracture toughness of the hybrid laminates. Further details are given in section 4.6.

Predicting the toughening effect provided by the introduction of the nanofibrous layers is challenging as it may depend on several factors, e.g. shape, diameter, porosity, arrangement, material, deposition, etc., of the interleaf [4,12]. The present study is aimed to explore the effect of PA6 nanofibre interleaves for achieving pseudo-ductility in hybrid composites by increasing the mode II fracture toughness of the layer interfaces and letting the CF/EP layer fragment without unstable delamination. This paper focuses on demonstrating the possibility of stabilising the originally unstable damage modes in hybrid composite laminates by promoting CF/EP fragmentation and enabling pseudo-ductility through interleaving nanofibrous layers.

## 3. Materials and methods

### 3.1. Preparation of nanofibrous layers

The nanofibrous layers were electrospun with an NS8S1600U needleless electrospinning machine (Elmarco s.r.o, Liberec, Czech Republic), designed for industrial production lines. The machine was equipped with eight 1.6 m wide stationary spinning wire electrodes. The polyamide 6 (PA6) to make the nanofibrous layers was Ultramide B27 (BASF, Czech Republic). PA6 was mixed with a solvent mixture (formic-acid and acetic-acid) (PENTA, s.r.o., Czech Republic) in the weight ratio of 2:1. We used two polymer concentrations in the prepared solutions: 8 wt% and 15 wt%, hereafter 8PA6 and 15PA6, respectively. The nanofibres were deposited to a substrate that was moving at speeds between 0.02 m/min to 0.8 m/min, depending on the desired areal weight of the nanofibrous layer (see Table 1).

All samples were electrospun onto silicon-coated paper to allow easy separation during further processing. The parameters in Table 1 indicate a few key differences in the nanofibres' basic properties: (i) 3–5 times higher speed is needed to get the desired areal weight with 15% concentration. (ii) The fibre diameter is more than two times higher in the case of the 15% solution. It can be concluded that the throughput is better for 15% PA6 concentration, but the quality (i.e. lowest possible fibre diameter) is worse.

### 3.2. Hybrid composite laminate manufacturing

The hybrid composite laminates were manufactured by laying up pre-impregnated sheets (prepregs) of IM7 carbon/913 epoxy and

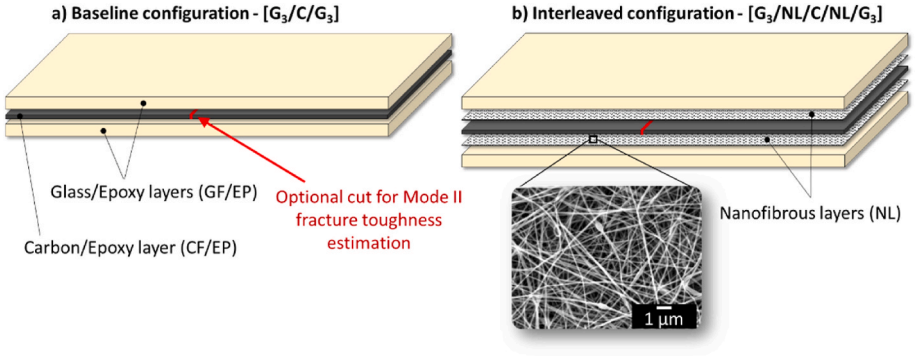


**Fig. 1.** Design layout of the (a) [$G_3$/C/$G_3$] (baseline) and (b) [$G_3$/NL/C/NL/$G_3$] (interleaved) unidirectional (UD), hybrid composite configurations. Nanofibres are inserted to the glass/epoxy (GF/EP) and carbon/epoxy (CF/EP) interfaces. The samples with central-cut CF/EP layer were used for estimating the mode II interlaminar fracture toughness of the hybrid laminates.

**Table 1**
Substrate speed of needleless electrospinning machine for different final areal densities of electrospun layers. All data are averaged and (CoV%) was calculated from 10 measurements.

| Targeted areal weight [g/m$^2$] | *Electrospinning solution PA6 concentration: 8 wt% (designation: 8PA6)* | | | *Electrospinning solution PA6 concentration: 15 wt% (designation: 15PA6)* | | |
|---|---|---|---|---|---|---|
| | Measured final areal weight [g/m$^2$] | Substrate speed [m/min] | Average fibre diameters [nm] | Measured final areal weight [g/m$^2$] | Substrate speed [m/min] | Average fibre diameters [nm] |
| 2 | 2.30 (7.7) | 0.20 | 108 (20.4) | 2.44 (8.6) | 0.80 | 267 (26.6) |
| 5 | 5.26 (11.0) | 0.12 | 103 (19.8) | 5.68 (11.8) | 0.36 | 243 (27.6) |
| 10 | 10.92 (12.4) | 0.05 | 121 (18.0) | 10.66 (8.8) | 0.22 | 280 (31.4) |

S-glass/913 epoxy, both supplied by Hexcel in 300 mm wide rolls. The mechanical properties of the materials are reported in Table 2. The resin films (RF) were also supplied by Hexcel in 300 mm wide rolls, and made with the same epoxy contained in the prepregs, i.e. 913 epoxy. The RFs had a nominal thickness of 30 μm, density of 1.23 g/cm$^3$ and an elastic modulus of 3.4 GPa.

The layup sequence used in the hybrid laminates is shown in Fig. 1. For the interleaved configurations, the nanofibrous layers were placed between the CF/EP and the GF/EP layers (see Fig. 1 (b)). Before the layup, the nanofibrous layers were dried for 4 h at 80°C. The hybrid laminates were put under vacuum after hand lay-up to improve the adhesion between the prepregs and the nanofibrous layers and remove residual air trapped between the plies during the layup process. The baseline configuration was manufactured without including the nanofibrous layers. The composites were cured in an OLMAR ATC 1100/2000 type autoclave at 125 °C and 0.7 MPa for 60 min, as recommended by the manufacturer of the prepregs. A vacuum pressure of −0.095 MPa was applied after sealing the vacuum bag and during the initial pressurisation phase in the autoclave. However, the vacuum was switched off after the pressure in the autoclave exceeded 0.12 MPa. The samples were fabricated by cutting the composite plates with a diamond cutting wheel. The nominal dimensions of the samples were 260 × 20 mm (nominal free length/width, respectively).

The estimated thermal residual strains due to the combination of two different type fibres (with different coefficients of thermal expansion) in the composite layers were 0.009% for the GF/EP layers and 0.024% for the CF/EP layer. Considering the i) low values of residual strains in the fibre-reinforced layers, ii) symmetrical layups which prevented the samples from residual bending deformations, and iii) consistent use of identical hybrid layups in all the configurations studied (i.e. the interleaved configurations differed only in the presence of nanofibrous layers, the number of CF/EP and GF/EP plies was the same as that of the baseline configuration), we decided to neglect the effect of thermal residual strains.

### 3.3. Mechanical test method

The uniaxial, quasi-static tensile tests on the hybrid composites were conducted on a computer-controlled Zwick Z250 universal electromechanic test machine, fitted with a regularly calibrated 250 kN load cell and 100 kN rated Instron 2716–003 type manual wedge action grips. The crosshead displacement speed was set to 5 mm/min. The presence of the high-strain S-glass/epoxy layers on the outsides of the hybrid laminates made the test of the specimens possible without using end tabs, as demonstrated in Ref. [23]. The ends of the specimens were covered with 50 mm long P80 grit size sandpaper pieces with the rough side turned to the specimen surface to prevent damage from the sharp nails of the grip faces while maintaining sufficient friction to avoid slippage. The present study analyses the damage modes in the CF/EP layer, i.e. presence of delamination and/or fragmentation. Therefore, all the tensile tests were interrupted at around 3% of strain (i.e. before the final failure of the hybrid composite, expected at around 3.5% strain) to prevent the final failure of the samples and preserve their integrity for further analysis (e.g. fragment length estimation and microscopy). Six specimens were tested for each material configuration. The strain was measured with a Mercury RT type optical extensometer system with a 5 MPixel Mercury Monet camera (Sobriety, Czech Republic). The gauge length of the specimens (between the markers tracked by the extensometer) was set to 120 mm.

### 3.4. Estimation of the mode II interlaminar fracture toughness and energy release rate at damage initiation

The Mode II interlaminar fracture toughness ($G_{IIC}$) in the hybrid configurations tested was characterised through a tensile test on the hybrid laminates made with a pre-cut and two-ply thick central layer to promote shear deformation between the (discontinuous) CF/EP layer and the (continuous) GF/EP layers (see Fig. 1). The delamination onset was taken as the stress before the load-drop during the tensile tests. The $G_{IIC}$ was calculated with formula 3.1 [11].

$$G_{IIC} = \frac{\sigma_{del}^2 h^2 E_c t_c}{8 E_g t_g \left(2 E_g t_g + E_c t_c\right)} \tag{3.1}$$

where $\sigma_{del}$ is the effective stress of the laminate at delamination, $h$ is the full thickness of the laminate, $E$ and $t$ are the elastic modulus and thickness of the CF/EP (subscript $c$) and GF/EP (subscript $g$) layers, respectively. Further details about the specimen configuration and the results are given in section 4.6. The energy release rate at damage initiation was evaluated with the same formula (i.e. 3.1) in the case of continuous CF/EP layer laminates but using the knee point stress instead

**Table 2**
Mechanical properties of the applied composite prepregs based on manufacturer's data.

| Prepregs | Nominal fibre areal density [g/m$^2$] | Fibre volume fraction [−] | Cured ply thickness [μm] | Tensile strain to failure [%] | Tensile modulus [GPa] | Coefficient of thermal expansion [1/K] |
|---|---|---|---|---|---|---|
| AGY Y-110 S-2 glass/913 epoxy | 190 | 0.49 | 153.8 | 3.7[a] | 45.6 | $3.20 \cdot 10^{-6}$[b] |
| Hexcel IM7 carbon/913 epoxy | 100 | 0.58 | 95.8 | 1.6 | 163.2 | $-0.103 \cdot 10^{-6}$ |

[a] Conservative strain limit based on our tests on pure S-glass/epoxy and hybrid specimens.
[b] Calculated from manufacturer's data given for 60% fibre volume fraction of the same fibre in epoxy matrix.

of the delamination stress. The knee point was determined as the intersection of lines fitted on the linear and the plateau part of the stress-strain curves, or taken as the peak point before any significant stress-drop as previously in Ref. [10].

### 3.5. Microscope analysis

The scanning electron microscope (SEM) analysis of nanofibrous layers and delaminated specimens was performed with a JEOL JSM 6380 LA (JEOL Ltd., Japan) equipment. The samples were sputter-coated with gold in a vacuum chamber to avoid static charging during imaging. Polished sections of the pristine and damaged samples were analysed with an Olympus BX51M type optical microscope (Olympus, Germany). For this purpose, representative parts of the investigated laminates were cut with a diamond wheel and then embedded in epoxy that was crosslinked for 24 h at ambient temperature. The resin blocks were polished with a Buehler Beta type machine with sandpapers (grit size P350 and P1000) and liquid suspensions of 9, 3 and 0.05 μm abrasive particle sizes. The thickness of the interlayers between the CF/EP and GF/EP composite layers was determined by manual measurements at minimum 50 positions and 10 micrographs for each configuration.

## 4. Results and discussion

This chapter summarises the experimental results of the tensile tests on the baseline and nanofibre interleaved hybrid composites. All the configurations tested are listed in Table 3 and Table 4.

**Table 3**
Results of the tensile tests on hybrid laminates containing 8PA6 nanofibrous layer (CoV in % expressed in brackets below the mean values, C-carbon/epoxy, G-glass/epoxy, RF-913 epoxy resin film). The nomenclature for hybrid composites containing nanofibrous layers was: e.g. 8PA6 – nanofibres made from 8%wt PA6 concentration in the electrospinning solution. The areal density of the nanofibrous layer is expressed by the last digits, e.g. 8PA6-2 = 2 g/m$^2$.

| Configuration | Baseline | Interleaved configurations [$G_3$/NL/C/NL/$G_3$] (NL refers to the Nanofibrous Layer) | | | | | |
|---|---|---|---|---|---|---|---|
| | | 8PA6-2 | 8PA6-2+RF | 8PA6-5 | 8PA6-10 | 8PA6-5+5 | 8PA6-10 + 10 |
| **Measured thickness** | 1.08 | 1.09 | 1.14 | 1.11 | 1.11 | 1.07 | 1.10 |
| **[mm]** | (1.9) | (2.1) | (2.1) | (2.0) | (1.9) | (2.1) | (2.8) |
| **Elastic modulus** | 58.0 | 56.6 | 54.5 | 55.7 | 56.8 | 56.5 | 54.8 |
| **[GPa]** | (2.7) | (2.6) | (2.0) | (3.8) | (1.5) | (4.1) | (4.2) |
| **Knee-point stress** | 1134[a] | 1124 | 1070 | 1099 | 1096 | 1074 | 1014 |
| **[MPa]** | (3.7) | (3.0) | (2.9) | (3.9) | (2.1) | (3.9) | (4.1) |
| **Knee-point strain** | 1.99[a] | 2.02 | 2.02 | 2.02 | 1.97 | 1.93 | 1.87 |
| **[%]** | (3.4) | (3.3) | (3.4) | (2.7) | (1.3) | (1.9) | (2.2) |
| **Strain energy release rate @knee-point** | 2.4 | 2.5 | 2.4 | 2.4 | 2.4 | 2.1 | 2.0 |
| **[kJ/m$^2$]** | (9.3) | (8.3) | (6.9) | (10.2) | (6.4) | (11.1) | (11.9) |
| **Average spacing between fragments** | - | 3.4 | 3.8 | 4.3 | 4.7 | 4.6 | 5.2 |
| **[mm]** | - | (16.2) | (15.9) | (15.4) | (15.0) | (17.1) | (16.3) |
| **Interfacial shear strength**[b] | 99.6[c] | 94.0 | 82.8 | 73.4 | 66.7 | 64.6 | 56.8 |
| **[MPa]** | (8.8) | (16.5) | (13.6) | (13.6) | (15.9) | (19.4) | (16.6) |
| **Mode II interlaminar fracture toughness**[d] | 1.8 | - | - | 2.9 | 3.9 | - | 4.7 |
| **[kJ/m$^2$]** | (7.4) | - | - | (8.1) | (6.6) | - | (7.8) |

[a] Evaluated from the load drop in the stress-strain curves of this configuration.
[b] Calculated through equation (4.1), analysing the spacing between CF/EP fractures.
[c] The value was calculated through the fragmentation analysis of a similar configuration containing 30 μm epoxy films, presented in Ref. [10].
[d] Measured on [$G_3$/NL/$C_2$/NL/$G_3$] laminates with a cut in the middle of the CF/EP layer.

**Table 4**
Results of the tensile tests on hybrid laminates containing 15PA6 nanofibrous layers (CoV in % expressed in brackets below the mean values, C-carbon/epoxy, G-glass/epoxy). The nomenclature for hybrid composites containing nanofibrous layers was: 15PA6 – e.g. 15PA6 – nanofibres made from 15%wt PA6 concentration in the electrospinning solution. The areal density of the nanofibrous layer is expressed by the last digits, e.g. 15PA6-2 = 2 g/m$^2$.

| Configuration | Baseline | Interleaved configurations [$G_3$/NL/C/NL/$G_3$] (NL refers to the Nanofibrous Layer) | | |
|---|---|---|---|---|
| | | 15PA6-2 | 15PA6-5 | 15PA6-10 |
| **Measured thickness** | 1.08 | 1.09 | 1.10 | 1.10 |
| **[mm]** | (1.9) | (2.2) | (2.2) | (1.9) |
| **Elastic modulus** | 58.0 | 56.8 | 57.0 | 57.3 |
| **[GPa]** | (2.7) | (3.1) | (2.7) | (1.5) |
| **Knee-point stress** | 1134 | 1122 | 1113 | 1108 |
| **[MPa]** | (3.7) | (2.8) | (2.3) | (2.2) |
| **Knee-point strain** | 1.99[a] | 1.97 | 1.96 | 1.96 |
| **[%]** | (3.4) | (4.0) | (2.2) | (1.6) |
| **Strain energy release rate @knee-point** | 2.4 | 2.4 | 2.4 | 2.4 |
| **[kJ/m2]** | (9.3) | (8.0) | (6.0) | (6.9) |
| **Average spacing between fragments** | - | 3.4 | 3.9 | 3.9 |
| **[mm]** | - | (15.3) | (21.5) | |
| **Interfacial shear strength**[b] | 99.6[c] | 89.5 | 78.0 | 76.1 |
| **[MPa]** | (8.8) | (17.6) | (21.9) | (2.4) |

[a] Evaluated from the load drop in the stress-strain curves of this configuration.
[b] Calculated through equation (4.1), analysing the spacing between CF/EP fractures.
[c] The value was calculated through the fragmentation analysis of a similar configuration containing 30 μm epoxy films, presented in Ref. [10].

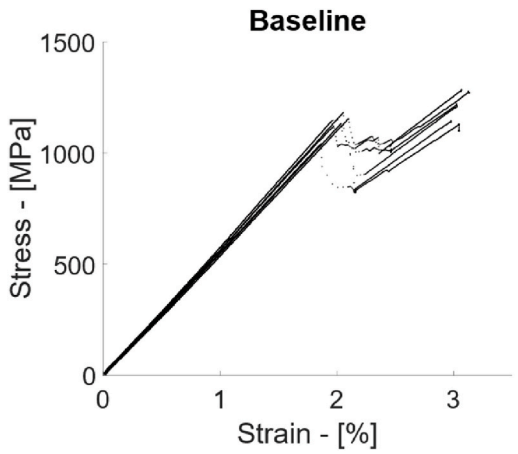


**Fig. 2.** Tensile stress-strain curves of the baseline configuration [$G_3$/C/$G_3$] [10].

### 4.1. Baseline hybrid composites

The mechanical behaviour of the configuration [$G_3$/C/$G_3$], considered as the *baseline*, has been previously studied and discussed in Ref. [10]. The tensile stress-strain curves are shown in Fig. 2. The average tensile elastic modulus of the series was 58 GPa up to the CF/EP layer fracture, which happened at around 1.9% strain. It is worthwhile to highlight the shape of the stress-strain curve, typical for hybrid composites with an unstable damage character. In fact, there is a stress drop corresponding to the first fracture of the CF/EP layer due to the sudden spread of delamination between the CF/EP and GF/EP layers of the specimens. Three out of six samples exhibited mixed damage patterns, with traces of fragmented and fully delaminated parts. This suggests that the baseline configuration was not far from the limit between unstable (but still gradual) and stable (i.e. fully pseudo-ductile) failure process. We obtained significantly higher strain values for the first CF/EP fracture than that quoted by the manufacturer for UD cured epoxy matrix composites (1.9% vs 1.6%) because the high strain GF/EP layers protected the CF/EP ply from stress-concentration induced premature failure near the grips [23].

### 4.2. Tensile tests on hybrid composites containing single polyamide 6 nanofibrous layers

The tensile test results on hybrid composites containing PA6 nanofibrous layers are reported in Fig. 3. Hereafter, we will refer to the interleaved configurations distinguishing the nanofibrous layers according to the percentage of PA6 used in the liquid solution for electrospinning, as follows: 8PA6, or 15PA6, together with the number indicating the areal density of the nanofibrous layer in g/m$^2$, e.g. 8PA6 – 2 for 2 g/m$^2$ nanofibrous layer made of a liquid solution containing 8 wt% of PA6.

The elastic moduli and the knee points of all the interleaved configurations were similar to those of the baseline configuration, i.e. average elastic modulus 56 GPa, knee-point at 1100 MPa and 1.98% strain (see Tables 3 and 4 – both tables report the results of the baseline series to make the comparison simple). Differently from the baseline series, there were specimens showing pseudo-ductile failure process in all the interleaved series. Each configuration showed a different grade of stability in the function of i) type of nanofibrous layer, i.e. 8PA6 or 15PA6, and ii) areal density of the nanofibrous layers, i.e. 2, 5 or 10 g/m$^2$. In general, the presence of the nanofibrous layers enabled the favourable fragmentation process of the CF/EP layer, generating the stable plateau visible in the stress-strain curves.

The stress-strain curves show that damage modes were highly dependent on the areal density of the nanofibrous layers. In fact, the hybrid configurations that registered more samples exhibiting fragmentation and pseudo-ductility were interleaved with thicker nanofibrous layers. Fig. 4 shows the appearance of typical samples from each configuration after the tests. The translucent GF/EP surface layers enabled the detection of CF/EP layer fractures (narrow light lines) and delamination (large or limited light areas). Both types of nanofibrous layers, i.e. 8PA6 and 15PA6, showed a similar trend for the configurations containing 2 g/m$^2$ and 5 g/m$^2$ (see (b), (c), (e), and (f) of Fig. 4). In (b) and (e) (i.e. 2 g/m$^2$ of both 8PA6 and 15PA6) the samples showed mixed damage modes, i.e. delamination + diffuse fragmentation of the

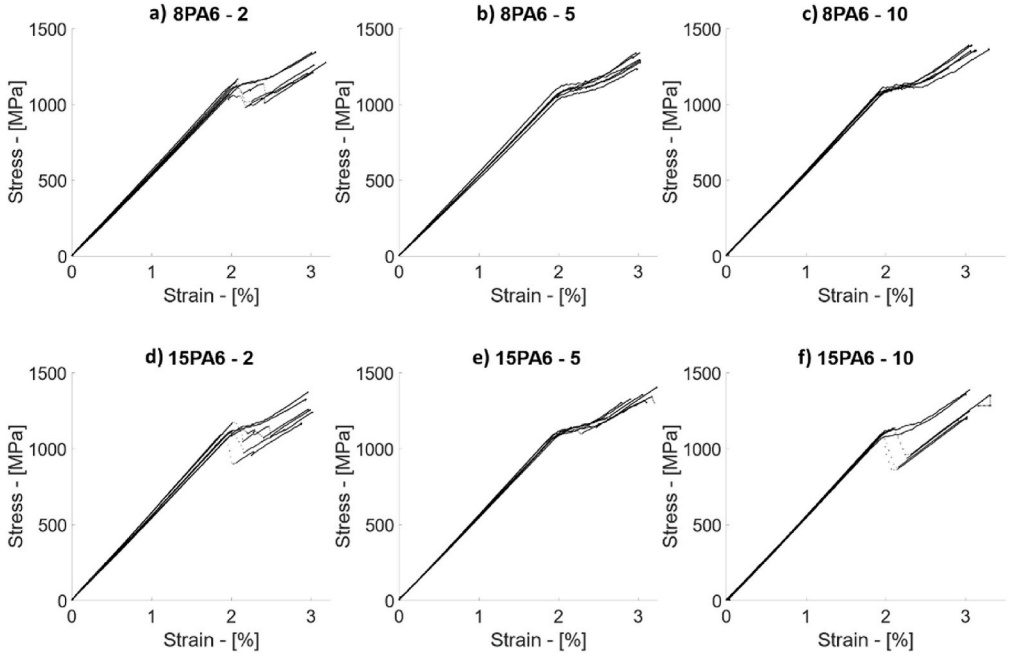


**Fig. 3.** Stress-strain curves of the 8PA6 and 15PA6 series, i.e. hybrid composites containing 8PA6 and 15PA6 nanofibrous layers with the areal weight of 2 g/m$^2$ in (a) and (d), 5 g/m$^2$ in (b) and (e), 10 g/m$^2$ (c) and (f).

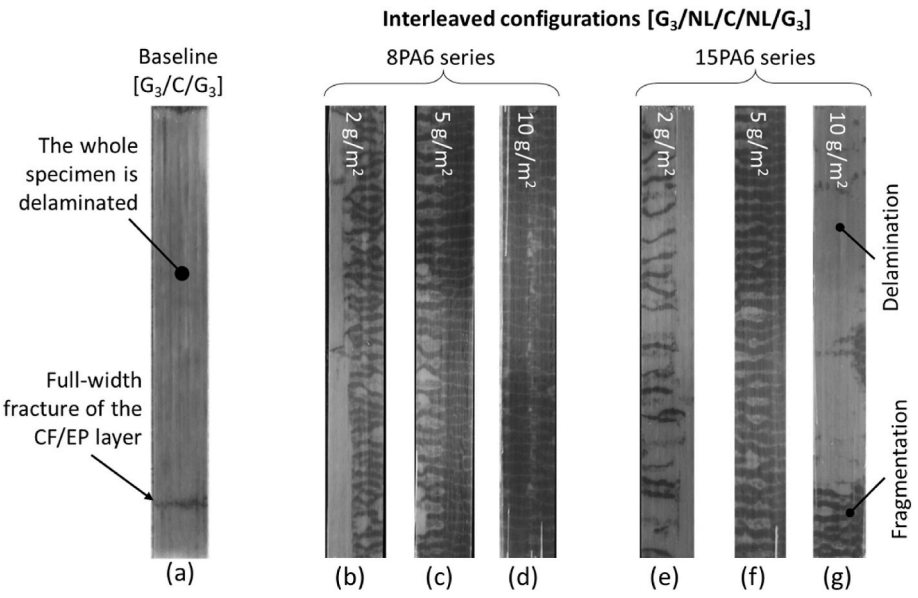


**Fig. 4.** Typical appearance of damaged hybrid composites at the end of the tensile tests: (a) baseline configuration and (b)–(g) samples containing nanofibrous layers.

CF/EP layer. The delamination, for these cases, spread suddenly and caused the stress drops registered in the stress-strain curves reported in Fig. 3 (a) and (d). However, two out of six samples of the 8PA6-2 series and three out of six samples of the 15PA6-2 series exhibited a pseudo-ductile behaviour. These samples were characterised by a progressive fragmentation of the CF/EP layer and delamination took place only locally near the CF/EP fractures.

The configurations containing 5 g/m$^2$ nanofibrous layers (i.e. 8PA6-5 and 15PA6-5) were characterised by stable and pseudo-ductile behaviour. All the samples showed fragmentation, and there was delamination only around the CF/EP fractures (see (c) and (f) of Fig. 4). The results obtained with the configurations containing 10 g/m$^2$ nanofibrous layers were not the same in the 8PA6 and 15PA6 series. The damage mode of the 8PA6-10 series was very stable (see Fig. 3 (c)), characterised by fragmentation of the CF/EP layer and very little delamination (see Fig. 4 (d)), a sign of a strong toughening effect at the CF/EP and GF/EP layer interfaces.

The stages of the two different damage processes, i.e. delamination + fragmentation and fragmentation only, are shown in Fig. 5 through two representative samples from the 8PA6-2 and 8 PA-10 series. Fig. 5 (a) shows that delamination occurred suddenly after the first fracture of the CF/EP layer and covered a significant part of the specimen. The other part of the specimen developed isolated fractures in the CF/EP layer and stable local delamination around them (i.e. fragmented, see stages a.2 and a.3). The samples with higher areal density of nanofibres showed a stable, progressive fragmentation process with multiple isolated CF/EP layer fractures and practically no delamination around them until high strain (see stages b.2 and b.3).

The 15PA6-10 series was mainly characterised by unstable delamination propagating at the first fracture of the CF/EP layer (see Fig. 3 (f)), although fragmented zones were also present in the samples (Fig. 4 (g)). Four out of six samples exhibited a sudden spread of delamination, registered after the first CF/EP layer fracture, together with fragmented regions. The results suggest that the thickness of the 15PA6 nanofibrous layer (i.e. 10 g/m$^2$) at the interfaces of the hybrid laminate may have exceeded a limit and started to degrade the mechanical properties of the

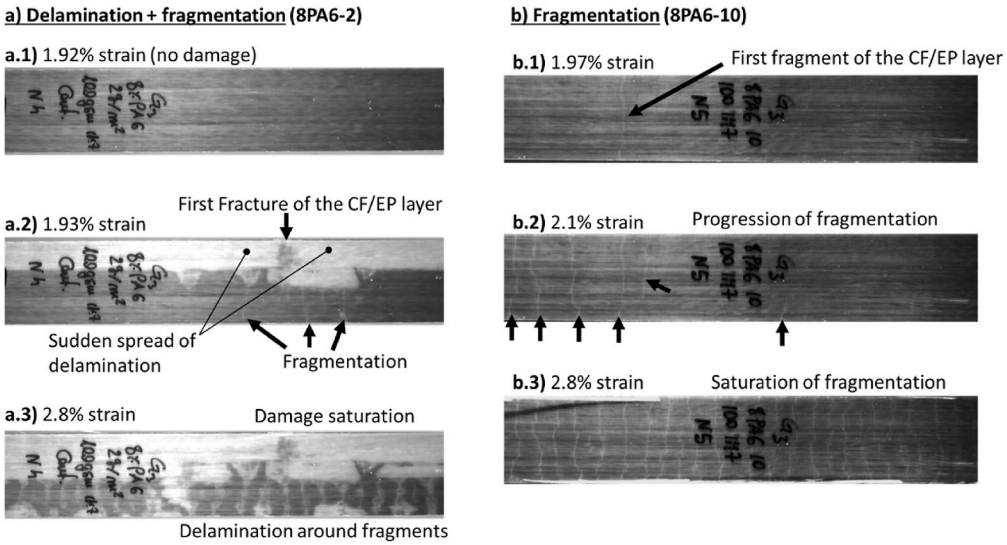


**Fig. 5.** Stages of damage propagation in representative samples from (a) 8PA6-2 and (b) 8PA6-10 series. The stages in (a) show the progression of delamination + fragmentation and in (b) fragmentation only.

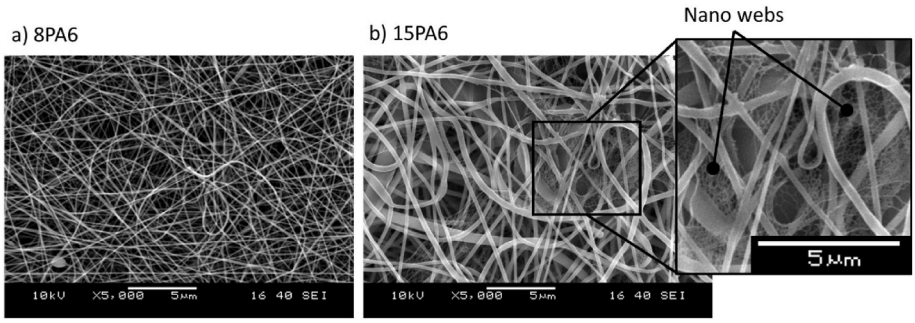


**Fig. 6.** Micrographs taken with the scanning electron microscope to compare the appearance of the two nanofibrous layers: 8PA6 in (a) and 15PA6 in (b).

interface. The presence of a thickness limit was already observed in the literature [4] with other types of nanofibres. In general, the two types of nanofibrous layers had different structure which may have played a role in the final performance of the interleaved hybrid composites: i) the diameter of the 15PA6 nanofibres is more than two times higher than that of the 8PA6 ones (see Fig. 6), which influences the specific surface area and possibly the impregnation with epoxy from the composite plies as well; ii) the SEM micrographs of the nanofibrous layers showed the presence of nanostructures similar to nets (called nano-webs in the literature) in the 15PA6 version (see Fig. 6 (b)), which might have affected the impregnation effectiveness of the nanofibrous layer. Further investigation is needed to fully understand the role of these structural parameters to the interfacial properties.

The analysis of the fragmentation in all configurations tested showed differences in the spacing between the fracture points of the CF/EP layers. The spacing may be considered an indicator of the shear strength of the interfaces containing nanofibres. In fact, the fracture spacing is dependent on the shear stress at the interface. This phenomenon is reflected in the widely used Kelly-Tyson equation [24]. The rearranged formula 4.1 based on [25] is derived similarly as the Kelly-Tyson equation but for flat layers and can be used for estimating the shear strength $\tau_s$ of the studied layer interfaces.

$$\tau_s = \frac{E_c \cdot \varepsilon_{c,f} \cdot t_c}{L_{ineff}} \qquad 4.1$$

$E_c$, $\varepsilon_{c,f}$ and $t_c$ are the elastic modulus, failure strain and thickness of the CF/EP layer, respectively. $L_{ineff}$ and $\tau_s$ are the ineffective length of the fibre-reinforced layer and the shear strength of the matrix, respectively [24]. $L_{ineff}$ after saturated fragmentation was estimated by dividing the free length of the specimen by the number of full-width fractures counted in the same section. The CF/EP fragments between two fractures do not fully take part in the load-bearing, i.e. there are large ineffective sections within the fragments. The length of the fragments depends on the shear forces the interfaces can transfer to the fragmented CF/EP layer (i.e. estimated shear strength of the interface) [25]. The higher spacing registered in hybrid composites containing nanofibrous layers indicated lower shear strength. However, the fragmentation instead of delamination and, in some cases, the absence of delamination indicated higher fracture toughness compared to that of the baseline configuration. We consider this higher mode II fracture toughness, due to nanofibrous layer interleaving, the feature of the interleaved composites that enabled pseudo-ductility. The shear strength based on the analysed fragment length for all the configurations is reported in Fig. 7. The baseline value (99.6 MPa) for no nanofibrous layer was estimated by applying the fragmentation analysis to the fragmented samples reported in Ref. [10] with the same lay-up sequence containing only extra epoxy at the interfaces. The lowering trend (diagrams (a) and (b)) indicates the negative influence of the areal weight of the nanofibrous layers on the shear strength especially for high areal weight. On the other hand, narrow delaminated areas observed around the CF/EP fractures in the laminates containing thicker nanofibrous layers (see Fig. 4 (b)–(d)) indicate higher delamination resistance (mode II fracture toughness) which is analysed further in section 4.6. This suggests that there is a trade-off between the interfacial shear strength and the mode II fracture toughness of the investigated hybrid laminates.

The results presented so far suggest, that the thickness of the interlayer between the CF/EP and GF/EP blocks in the hybrid laminates play an important role in their strength and delamination resistance (i.e. mode II fracture toughness), therefore this structural parameter was investigated in depth. The micrographs and diagrams of Fig. 8 typical of all tested configurations (including 15PA6 types) clearly show that the presence of thicker nanofibrous layers between the CF/EP and GF/EP layers made the interlayers thicker.

A linear fit to the data points of Fig. 8 f) and g) would not hit the origin, which suggests that there is a finite thickness of the interlayer between the composite plies (around 15 µm) even if we do not interleave any nanofibrous layer. This makes good sense, given that misalignment of fibres at the surface of prepreg plies is a common artefact of manufacturing and handling, which can easily induce a small "gap" between the densely packed fibrous layers to be filled with resin from the bulk of the plies.

The markers corresponding to the thickness of interlayers produced by the 2 g/m$^2$ nanofibrous layers seem to stand out especially in case of the 15PA6 series, probably because the gap between the composite

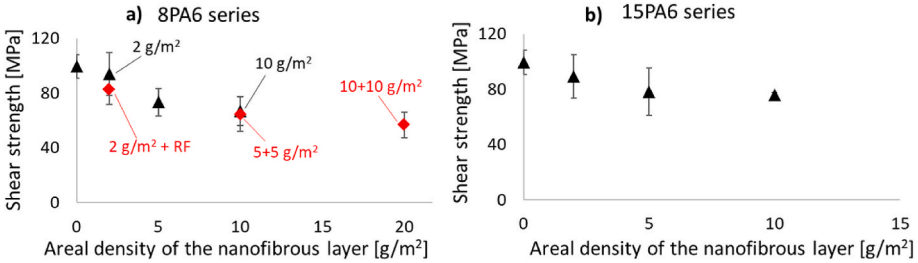


**Fig. 7.** Estimations of the interfacial shear strength in the function of the areal weight of the 8PA6 (a) and 15PA6 (b) nanofibrous layers interleaved in hybrid composites. The red data points in (a) are related to the "special" configurations that contain multiple nanofibrous layers (i.e. 5 + 5 and 10 + 10 configurations) or combined with resin films (i.e. 2 g/m$^2$ + RF).

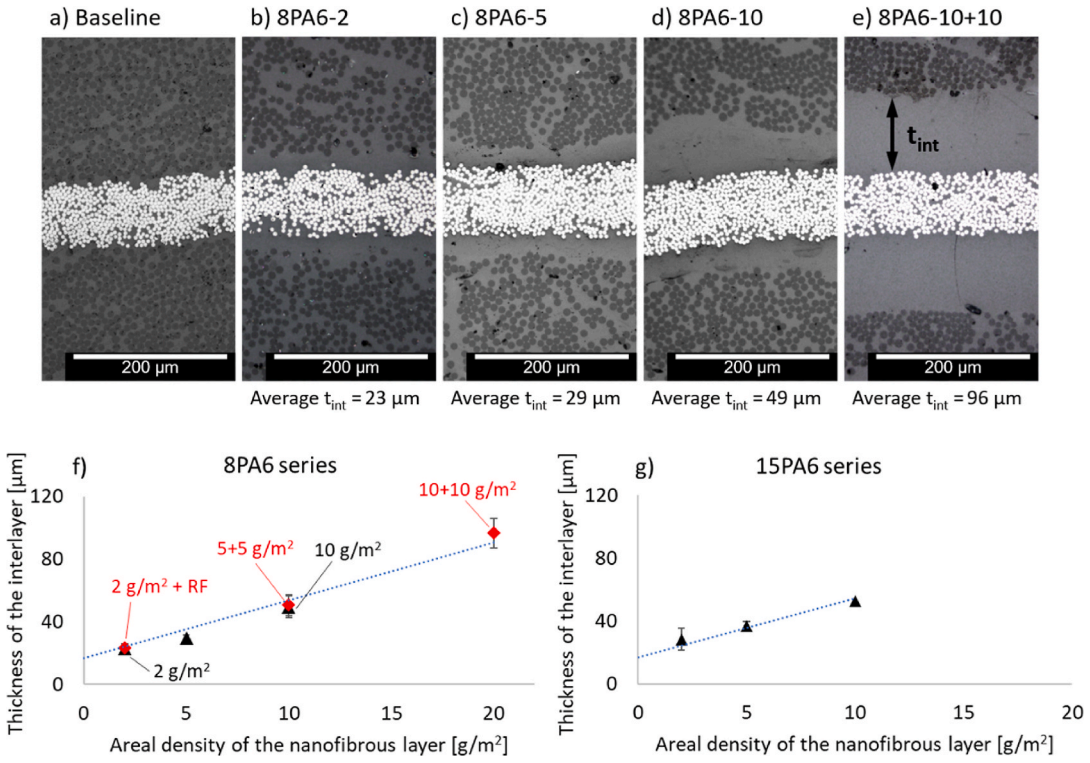


**Fig. 8.** Cross-sectional optical microscope analysis of the undamaged hybrid samples: [$G_3$/C/$G_3$] (baseline) (a) and laminates containing 8PA6 nanofibrous layers (b)–(e). The concentration of the nanofibrous layers is expressed by the name of each configuration (e.g. 8PA6-2 for 8% PA6 – 2 g/m$^2$). The graphics in (f) and (g) plot the interlayer thicknesses against the areal density of the interleaved nanofibrous layers.

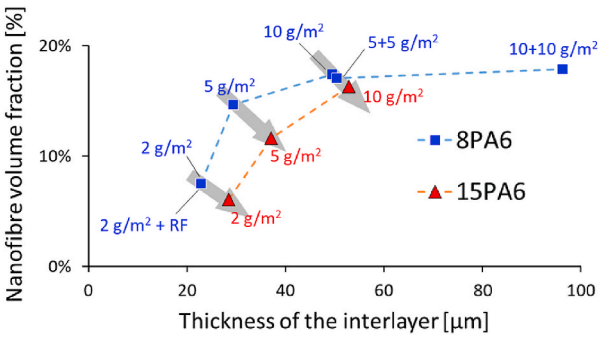


**Fig. 9.** Theoretical volume fraction of the nanofibres in the interlayers in function of the thickness of the interlayer between the CF/EP and GF/EP layers.

layers was largely magnified by the addition of any small "space holder" (i.e. the nanofibrous layer). At higher nanofibrous layer areal densities, the small amount of the extra resin between the layers does not seem to play a significant role in the resulting interlayer thickness. In general, we concluded that there is a roughly linear trend between the areal density of the interleaved nanofibrous layers and the resulting interlayer thicknesses.

We also calculated the theoretical nanofibre volume fraction in the interlayers by considering the nominal areal weight of the nanofibrous layers and the thickness of the interlayer measured as per Fig. 8. The values of calculated nanofibre volume fractions are reported in Fig. 9 for all interleaved configurations. The data reported in the diagram allows us to draw the following conclusions: i) thinner interlayers tend to have lower nanofibre volume fraction, most probably because the non-uniform border of the micro-fibrous layers (due to e.g. some mis-aligned fibres) are holding a small gap between the composite plies and the nanofibrous layers which is filled with matrix (see Fig. 11); ii) the nanofibre volume fraction exhibited a saturation limit around 20%, meaning that we can increase the thickness of the interlayer, but the fibre volume fraction will not change any further; iii) with the same areal weight (e.g. 2 g/m$^2$), the fibre volume fraction of 15PA6 nanofibres is lower than that with 8PA6 nanofibres. This might be the consequence of the lower diameter 8PA6 fibres being less stiff, so the layer is probably easier to be compacted by the autoclave pressure applied; iv) the configurations 8PA6-2 and 8PA6-2+RF showed the same fibre volume fraction and interlayer thickness. It indicates that the thickness of the interlayer primarily depends on the areal density of the nanofibrous layer and can be precisely controlled through it. It is concluded that the excess epoxy introduced with the resin film migrated in the surrounding composite plies.

The shear strength values decreased with interlayer thickness, while the failure mode became more stable for thicker interlayers in general (primarily for 8PA6 types). This sounds controversial at a glance, but we found sensible explanation for the trade-off between shear strength and delamination resistance: (i) The shear load bearing (or transferring) capacity of an interface is expected to reduce if thicker interlayers made of a rather low strength material is introduced between stiff and strong blocks (decreasing shear strength with interlayer thickness); (ii) The delamination resistance (or fracture toughness) is usually increased by limited stiffness at the interface e.g. provided by a thick and compliant interlayer, as it can tolerate rather high relative displacements of the surrounding blocks without experiencing too high shear strain. It can be demonstrated by simple geometric tools (see Fig. 10 (a) and (b) and formula 4.2), that a thicker block of material (i.e. an interleaved interface) goes under proportionally lower shear strain (i.e. angular distortion) due to the same relative displacement of the surrounding blocks (i.e. composite layers) than a thinner one.

$$\gamma = tg\theta = \frac{\Delta x}{t_{int}} \qquad 4.2$$

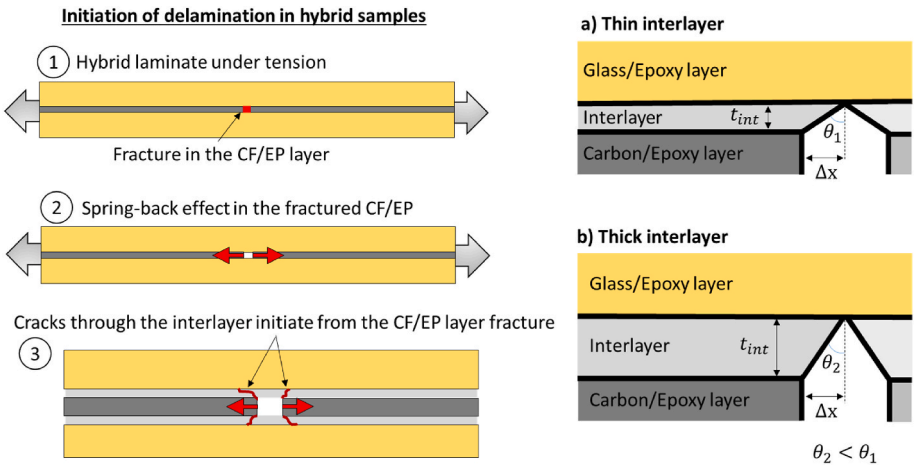


**Fig. 10.** Schematic representation of the shearing mechanism generated in the interlayer after the fracture of the CF/EP layer. In the thin case (a), higher shear deformation is generated in comparison to the thick case (b).

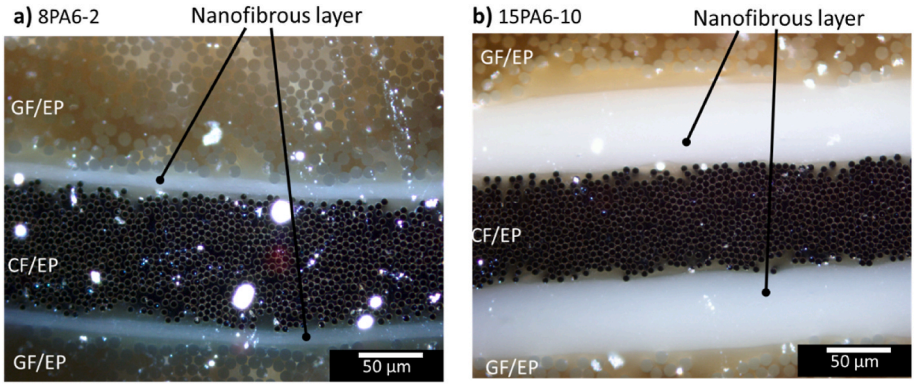


**Fig. 11.** Cross-section analysis of the samples from the (a) 8PA6-2 and (b) 15PA6-10 series. The samples highlight the presence of nanofibrous layers infiltrated with epoxy between the CF/EP and GF/EP layers. (The bright spots are due to light reflection).

Where $\gamma$ is the shear strain, $\theta$ is the angular distortion, $\Delta x$ is the shear displacement and $t_{int}$ is the thickness of the interlayer. This simple phenomenon is particularly useful in extending the damage process zone and knock down singular shear stresses at the tips of mode II interlaminar cracks. Therefore, we consider this geometric effect the key toughening mechanism governing the stable damage process registered in most of the interleaved hybrid laminates.

### 4.3. Microscope analysis

The pseudo-ductility registered in the developed interleaved hybrid composites is attributed to the presence of the nanofibrous layers at the CF/EP and GF/EP interfaces, although their direct effect on the mechanical behaviour of the hybrid samples and the CF/EP fragmentation needs further investigation. The cross-section analysis documented in Fig. 8 clearly show the thickness increase of the interlayers that separate the CF/EP and GF/EP layers. The presence of a thick and compliant interlayer between the fibre reinforced layers is expected to allow higher displacement of the surrounding CF/EP and GF/EP layers without triggering delamination, therefore it is tougher in mode II.

The nanofibrous layers between the CF/EP and GF/EP layers are highlighted in Fig. 11. The figure clearly confirms the existence of the nanofibrous layers in the cured composite and shows that they are infiltrated by the epoxy matrix of the composite layers during the cure cycle. The nanofibrous layers act as space holders between the CF/EP and GF/EP layers. The thickness of the interlayer consisting of the epoxy infiltrated nanofibrous layer is well controlled by the areal weight of the interleaves.

In order to investigate the fracture morphology of different specimen types, a scanning electron microscope (SEM) analysis was performed, but on the delaminated samples only, as the fragmented ones had parts of their layer interfaces which were still bonded. In fact, it was impossible to open up the layer interfaces of fragmented specimens without introducing further delamination to them (which are not possible to distinguish during imaging and could easily compromise the validity of the results), therefore the fragmented parts could not be investigated under the SEM. The analysis of the fractured matrix in delaminated samples showed the presence of nanofibres, as shown in Fig. 12 (a) and (b). The raw material of the nanoveils (PA 6) has a melting temperature above 200 °C, therefore it is not expected to melt and change its appearance during the cure cycle of the hybrid laminates at 125 °C. Fig. 9 a) and b) confirms, that the nanofibres were not affected by the cure cycle and the infiltration by epoxy. Fig. 12 (c), (d) and (e) show the CF/EP side of the delaminated faces of the baseline, 8PA6-2 and 15PA6-2 samples. No significant difference was noticed in the delamination surface morphology that might be highlighted. In all three cases, the patterns observed in the fractured resin were similar to hackles, typical of shear fracture of epoxy. Furthermore, it is worthwhile to highlight that we did not notice any preferential trend in the interlayer to remain attached to the CF/EP or GF/EP side of the interface.

The fragmented zones of the pseudo-ductile samples were studied on longitudinal-sections with optical microscope. The results are reported in Fig. 13. The micrographs focus on the 8PA6 series, but we registered similar patterns of the cracks in the 15PA6 series. The cracks generated

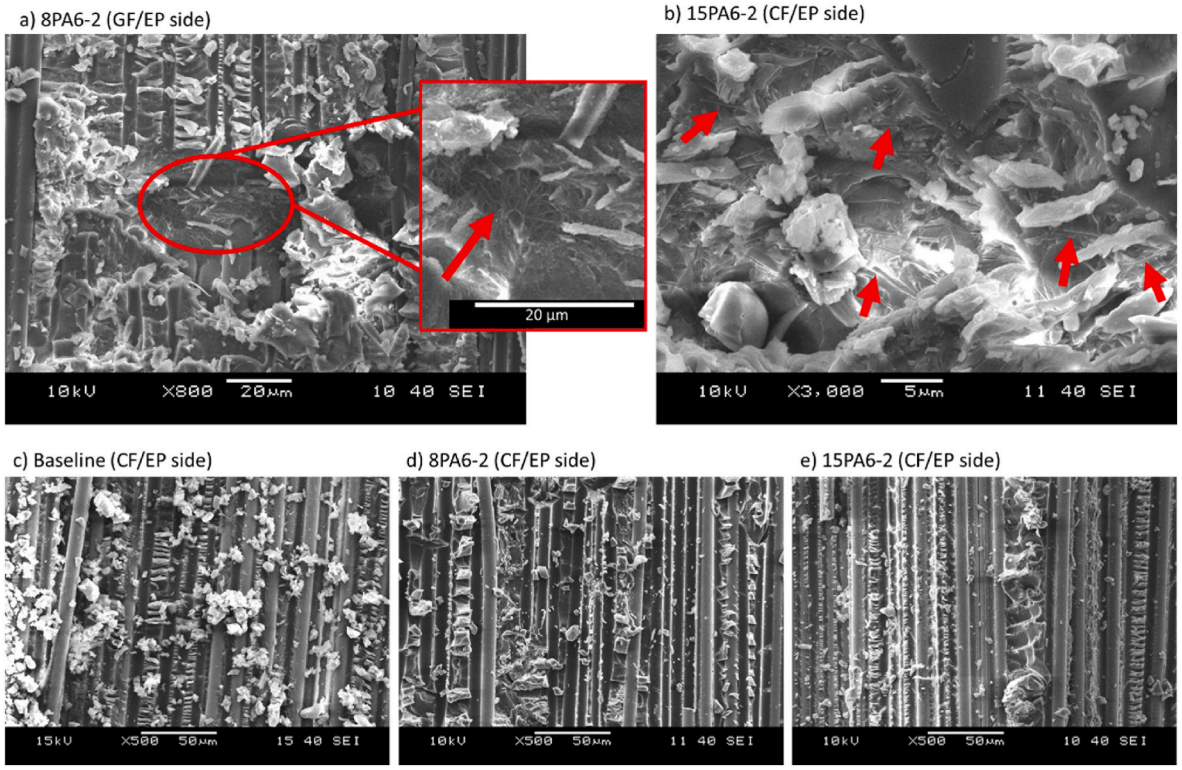


**Fig. 12.** SEM analysis of the delaminated surfaces of 8PA6-2 ((a) and (d)), 15PA6-2 ((b) and (e)) and baseline specimens (c). Parts (a) and (b) show the presence of nanofibres in the cured laminates, (c)–(e) compares the delamination fracture morphology of different samples.

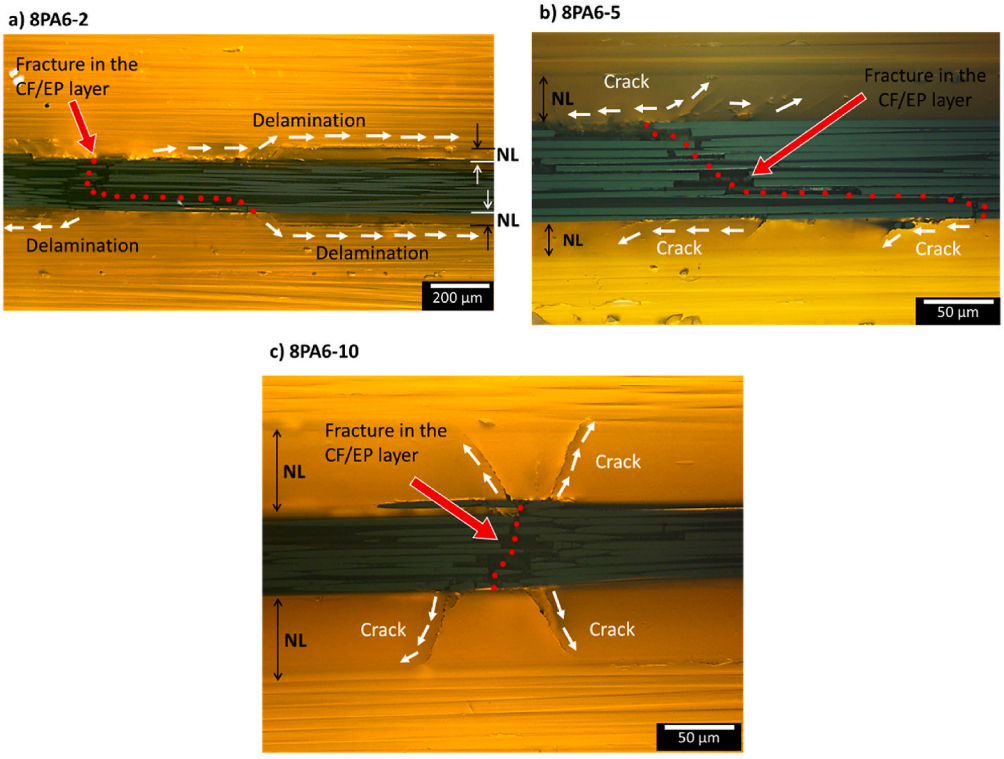


**Fig. 13.** Optical microscope analysis of the hybrid samples: longitudinal sections of the fragmented samples from (a) 8PA6-2, (b) 8PA6-5 and (c) 8PA6-10 configurations. (NL = nanofibrous layer).

after the fracture of the CF/EP layer show a propagation trend that is dependent on the nanofibrous layer areal density. The cracks in the configuration 8PA6-2 (Fig. 13 (a)) propagate across the interlayer containing nanofibres and along the GF/EP interface. The extended delamination crack path (up to the mm scale) is in agreement with the delamination pattern observed visually from the outer surface of the

sample (see Fig. 4 (b)). In case of 8PA6-5 and 8PA6-10 (see Fig. 13 (b) and (c), respectively), the delamination cracks are significantly shorter and arrested within the nanofibrous interlayers. We concluded that the typical crack propagation patterns are affected by the thickness of the interlayer and therefore by the areal density of the interleaved nanofibrous layer. In agreement with Fig. 4 (c) and (d), the delamination cracks in 8PA6-5 and 8PA6-10 are more and more suppressed in function of the areal density of the nanofibrous layer.

### 4.4. Synergetic effect with extra epoxy films

The configuration 8PA6-2 exhibited pseudo-ductility only in two out of six samples of the series. Since stable behaviour was obtained with 5 and 10 g/m$^2$ of the same nanofibrous layers, we concluded, that the areal weight of nanofibres at the composite interfaces was not high enough to enable the toughening mechanisms necessary to supress delamination and promote fragmentation of the CF/EP layer. Our previous study [10] on similar hybrid composites showed that extra 34 g/m$^2$ (approx. 30 μm of thickness) Hexcel 913 resin film interleaves promoted a slight decrease of the overall fibre volume fraction, resulting in a more stable behaviour than that of the baseline. Here, we wanted to check if the combination of the same resin films and nanofibrous layers may create synergetic, beneficial toughening effects leading to pseudo-ductility. The results of the tensile tests on baseline containing resin films (RF) [10], 8PA6-2 and 8PA6-2+RF are reported in Fig. 14. The configuration containing a combination of nanofibres and resin films (8PA6-2+RF) generated a stable pseudo-ductile behaviour unlike the other two configurations with single interleaving approaches, where we had mixed failure modes. The differences in the damage modes were visible from the appearance of the samples after the tensile tests (see Fig. 15). The 8PA6-2+RF showed fragmentation of the carbon layer and signs of local delamination around the fragments (Fig. 15 (b)), contrarily to the 8PA6-2 series, which had large delaminated regions (Fig. 15 (a)).

The thickness measurements at the CF/EP and GF/EP interfaces (see cross-sections in Fig. 15) revealed similar values for both configurations. However, there was an overall increase in the hybrid laminate thickness, from 1.11 mm for 8PA6-2 to 1.14 mm for 8PA6-2+RF. The total of about 45 μm thickness increase correlates well with the nominal thickness of two resin film layers (50 μm). The micrographs of Fig. 15 does not show a clear effect of the extra resin layers on the interlayer thickness and local fibre volume fraction next to them, which indicates that most of the resin flowed into the fibre reinforced layers and distributed uniformly, decreasing the overall fibre volume fraction slightly in the GF/EP layers (from 49% to 46% which is hard to detect visually). Nevertheless, any decrease in the fibre volume fraction is expected to contribute to higher mode II fracture toughness.

Further investigation is needed to draw solid conclusions about the factors that have promoted more stable failure mode in the 8PA6-2+RF specimens compared to the 8PA6-2 configuration.

### 4.5. Possibility of stacking multiple nanofibrous layers

The positive trend found in the 8PA6-5 and 8PA6-10 configurations led us to explore the possibility to achieve pseudo-ductility with even thicker nanofibrous layers at the interfaces in our hybrid composites. There are manufacturing issues related to the electrospinning of too thick nanofibrous layers, e.g. areal densities above 10 g/m$^2$. Electrospinning nanofibres to form high areal density layers may present separation problems due to reduced adhesion to the supporting material (i.e. silicon paper), if the thicker layer becomes too heavy. At the same time, too low velocities of the substrate material leading to higher nanofibrous layer areal density can cause non-uniform distribution of nanofibres and thus increase the inhomogeneity of the areal weight in the resulting layers. Higher areal density nanofibrous layers at the interfaces can however be

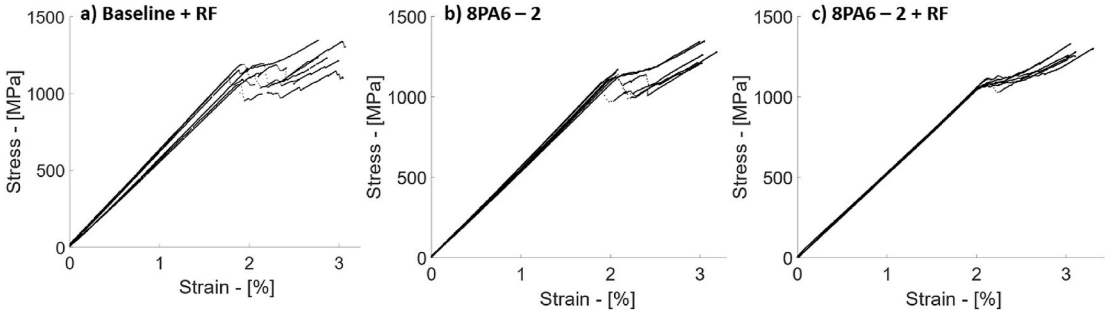


**Fig. 14.** Stress-strain curves of tensile tests on hybrid composites containing 30 μm resin film (RF) [10] (a), 8PA6-2 nanofibrous layers (b) and 8PA6-2 + 30 μm resin film (i.e. 8PA6-2+RF) (c).

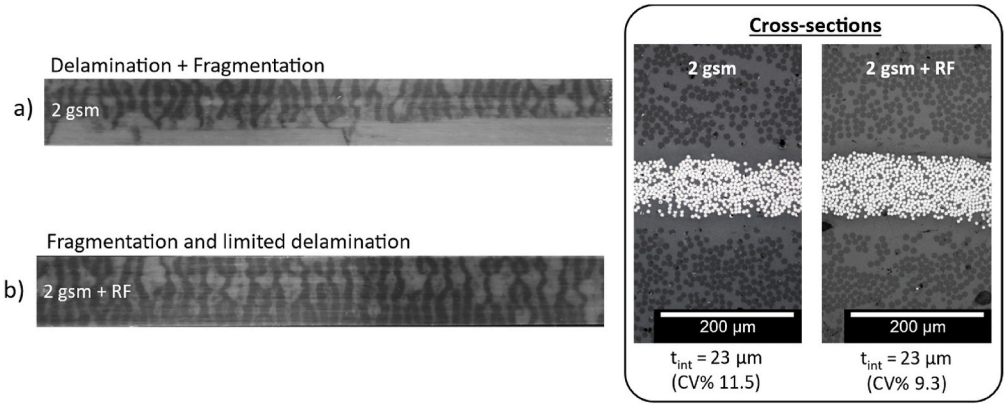


**Fig. 15.** Typical appearance of damaged hybrid composites interleaved with 8PA6-2 nanofibrous layers (a) and 8PA6-2 + resin film (i.e. 8PA6-2+RF) (b) after the tensile tests. The cross-sections highlight the similar interlayer thickness ($t_{int}$) for the two configurations.

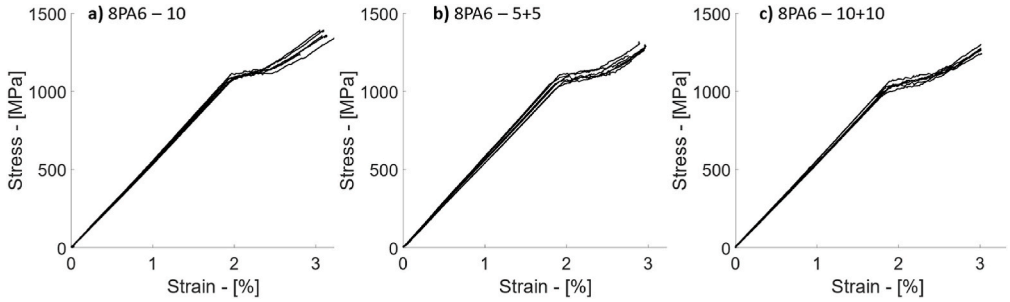


**Fig. 16.** Stress-strain curves of three 8PA6 series, i.e. hybrid composites containing 8PA6 nanofibrous layers with 10 (a), 5 + 5 (b) and 10 + 10 (c) g/m$^2$ areal density.

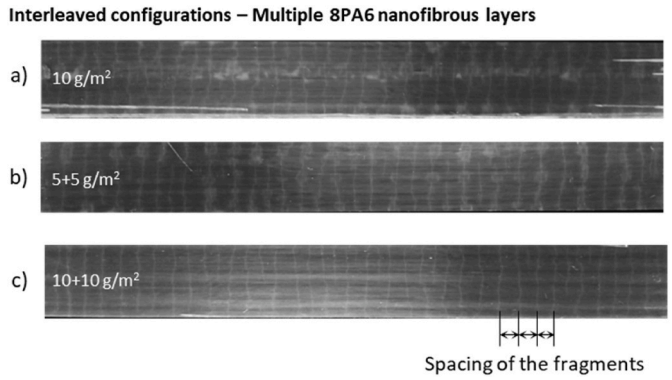


**Fig. 17.** Appearance of damaged hybrid composites containing 8PA6 nanofibrous layers with (a) 10, (b) 5 + 5 and (c) 10 + 10 g/m$^2$ areal density.

achieved by stacking multiple nanofibrous layers. To assess the feasibility of this approach, an experiment on the configuration 8PA6–5+5 was executed, stacking two layers of 8 wt% PA 6 nanofibres with 5 g/m$^2$. Nominally, the two configurations, 8PA6-10 and 8PA6–5+5, should be considered analogous because the nanofibrous layers have the same total areal weight at the composite layer interfaces. The stress-strain curves of the two configurations are reported in Fig. 16 (a) and (b).

Although the 8PA6–5+5 series shows a slightly higher scatter in the plateau stage, the performance of the configurations was similar in terms of damage modes. Both configurations showed fragmentation of the CF/EP layer and only traces of delamination around the fragments, as shown in Fig. 17 (a) and (b).

The fragmentation analysis revealed similar spacing between fragments and shear strength values at the interfaces (see Table 3). The configuration with 10 + 10 g/m$^2$ (nominally 20 g/m$^2$) of 8PA6 also provided a stable behaviour. The resulting stress-strain curves were similar to the ones obtained with the other configurations. The difference is only visible in the final appearance of the samples after the tests. The 8PA6–10 + 10 series did not show traces of delamination in the samples, i.e. fragmentation only (see Fig. 17 (c)). It indicates a superior resistance against delamination (i.e. high $G_{IIC}$) in comparison to the other configurations interleaved with thinner layers of 8PA6 nanofibres. The spacing between CF/EP fractures registered in this configuration provided a further confirmation of the trend found previously. In fact, the 10 + 10 configuration generated fragmentation with an average spacing of 5.2 mm (see Table 3), which is higher than the previous values. Consequently, the estimated value of the shear strength at the interfaces is the lowest while delamination resistance seems to be the highest registered in this study. The evolution of the damage modes, in relation to the areal density and the calculated shear strength at the interfaces, indicates that there is a trade-off between shear strength and delamination resistance. The results suggest the need to find the optimal balance between shear strength and toughness, to enable pseudo-ductility in hybrid composite materials.

### 4.6. Mode II interlaminar fracture toughness of interleaved hybrid composites

The pseudo-ductility obtained in the hybrid configurations containing 8PA6 nanofibrous layers indicates a variation in the interlaminar fracture toughness of the hybrid laminate in function of the areal density of the nanofibrous layers interleaved. A test campaign was performed to quantify the improvement of the mode II interlaminar fracture toughness ($G_{IIC}$) in the interleaved hybrid laminates. To promote mode II deformation at the CF/EP and GF/EP interfaces, the central CF/EP layer of the hybrid laminates was pre-cut before lay-up and made discontinuous. This way, the discontinuity promoted the desired shear deformation at the composite layer interfaces during the tensile tests of the hybrid laminates. The method was already used in Ref. [11] to measure the $G_{IIC}$ in thermoplastic film interleaved composites. Since the discontinuous version of the baseline configuration did not produce high enough energy release rate to promote delamination, we decided to add

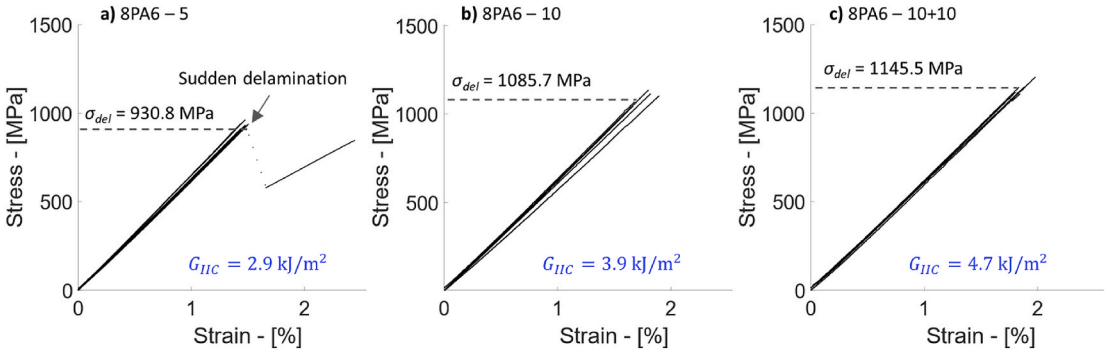


**Fig. 18.** Stress-strain curves of the Mode II fracture toughness test on composites containing 5 (a), 10 (b), and 10 + 10 g/m$^2$ (c) nanofibrous layers.

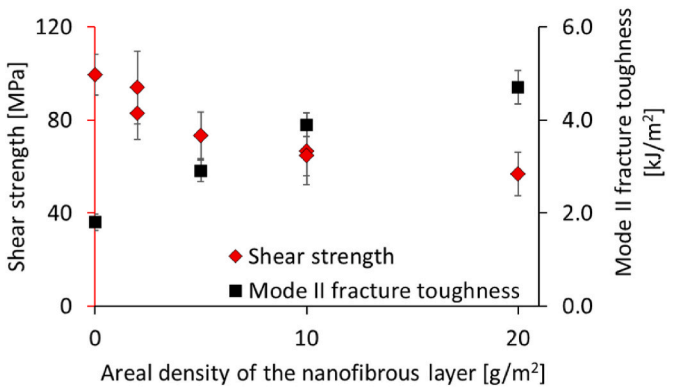


**Fig. 19.** Comparison of the shear strength and mode II fracture toughness ($G_{IIC}$) results in function of the areal density of the 8PA6 nanofibrous layers interleaved in the tested hybrid laminate configurations.

one more CF/EP ply to have the closest possible design [$G_3$/NL/$C_2$/NL/$G_3$] which is still suitable for the test (i.e. delaminates from the cut before the CF/EP layer would fracture).

Fig. 18 reports the stress-strain curves of the tensile tests to characterise the $G_{IIC}$ in the hybrid composites containing 8PA6-5, 10 or 10 + 10 g/m$^2$ nanofibrous layers. The stress/strain curves are linear (except one) because the video extensometer stopped recording the strain at the significant load drop corresponding to the sudden delamination (i.e. the marker paint came off the specimens). The delamination onset in the 8PA6-5 registered was around 930 MPa, which results in a $G_{IIC}$ equal to 2.9 kJ/m$^2$, 60% higher than that of the baseline configuration i.e. 1.8 kJ/m$^2$ [10].

The delamination stresses we registered in the configurations of hybrid composites interleaved by 10 and 10 + 10 g/m$^2$ nanofibrous layers were even higher than that obtained with the 5 g/m$^2$ nanofibrous layer. At higher areal densities, the delamination onset shifted towards higher values of stress (see Fig. 18 (b) and (c)). The higher delamination stress indicates higher Mode II interlaminar fracture toughness, according to equation (3.1). The $G_{IIC}$ of the other two configurations was 3.9 kJ/m$^2$ for the 10 g/m$^2$ configuration, and 4.7 kJ/m$^2$ for 10 + 10 g/m$^2$ configuration (see Table 3). The values of $G_{IIC}$ found in all the interleaved configurations were significantly higher than i) the $G_{IIC}$ measured in the baseline configuration and ii) higher than the energy release rate at the fracture of the CF/EP layer in the continuous hybrid configurations (see Table 3). The increasing $G_{IIC}$ in function of nanofibrous layer areal density confirms the trade-off between interfacial shear strength and fracture toughness of nanofibrous layer interleaved hybrid composites mentioned in section 4.2. The trade-off is highlighted in Fig. 19, where the shear strength and the $G_{IIC}$ are plotted together in function of the areal density of the nanofibrous layers. The obtained results confirm that the nanofibrous layers interleaved between the composite layers in our hybrid laminates largely increased the mode II fracture toughness of the interfaces, suppressed delamination around the multiple fractures of the CF/EP layer and therefore promoted further CF/EP layer fragmentation and pseudo-ductile failure mode.

## 5. Conclusions

An effective interleaved architecture was proposed for pseudo-ductile hybrid composites in this paper. Interleaving nanofibrous layers in hybrid composites was beneficial for promoting stable damage modes and pseudo-ductility in hybrid laminates made with cost-effective standard thickness carbon/epoxy (CF/EP) low-strain layers. The baseline configuration, i.e. without interleaves, had an unstable damage mode dominated by catastrophic delamination of the CF/EP layer. We examined the effect of two types of nanofibrous layers produced by electrospinning from liquid solutions with 8 wt% and 15 wt% of polyamide 6 (i.e. 8PA6 and 15PA6, respectively). The nanofibrous layers differed in the fibre diameters (8PA6 nanofibres were lower in diameter than 15PA6) and in the morphology (15PA6 contained nano webs between the fibres). Moreover, the toughening effectiveness was evaluated in the function of the areal weight of the applied nanofibrous layers.

In general, both types of nanofibrous layers were beneficial for stabilising the damage process of the hybrid laminates, but better results were obtained with the 8PA6 types, probably due to the lower fibre diameter and better wettability. The 8PA6 nanofibrous layers enhanced the mechanical performance of the hybrid laminates by generating pseudo-ductility. The improvement of the damage modes has been assessed qualitatively and associated with a reduced presence of delamination, which was visible from the outer surface of the tested samples and less drops on the stress-strain diagrams. Hybrid laminates with thicker nanofibrous layers were more delamination resistant and their damage mode was dominated by fragmentation of the CF/EP layer and local delamination around the fractures only. In particular, the series with thick 8PA6 nanofibrous layers (e.g. 20 g/m$^2$) showed fragmentation with no delamination around the CF/EP fractures in the samples. Higher nanofibrous layer areal density values were achieved by stacking two layers of nanofibres together. This original approach makes the use of thicker nanofibrous layers possible and allows to further increase the mode II interlaminar fracture toughness ($G_{IIC}$) in hybrid composites. An interesting trade-off was observed between the shear strength and the $G_{IIC}$ of the 8PA6 specimen types in function of the interlayer thickness. Thicker interlayers between the CF/EP and GF/EP layers generated by high areal density nanofibrous layers resulted in decreased estimated interlaminar shear strength but provided superior mode II fracture toughness ($G_{IIC}$) up to 4.7 kJ/m$^2$ and showed only traces of delamination in the fragmented samples.

The series of samples interleaved by 15PA6 nanofibrous layers displayed pseudo-ductile behaviour in hybrid composites only with the areal density of 5 g/m$^2$. The failure mode of 15PA6-10 samples was mainly unstable. Further study is required to understand the reason for the less stable damage processes experienced in the 15PA6 series.

The microscope analysis confirmed the presence of individual nanofibres (SEM images) and the whole epoxy infiltrated nanofibrous layers in the cured composite samples (optical microscopy). This suggests that the interleaves were not significantly affected by the applied temperature (well below the melt temperature of PA6) and the chemical formulation of the epoxy in the prepreg plies. The micrographs also reveal the important space-holding and interlayer thickness controlling role of the nanofibrous layers between the composite layers. The microscope analysis showed that thicker interlayers prevented delamination cracks from extensive propagation and in case of 8PA6-10, delamination cracks were suppressed.

$G_{IIC}$ estimation tests on the interleaved hybrid specimens with discontinuous CF/EP layer confirmed the toughening effect of the applied nanofibrous layers. The results showed that the additional mode II fracture toughness of the tested interleaved interlayer hybrid composite laminates was high enough to promote fragmentation of the CF/EP layers. The $G_{IIC}$ was significantly increasing with the areal density of the nanofibrous interleaves in the case of 8PA6 nanofibrous interlayers, i.e. from 1.8 kJ/m$^2$ (baseline) up to 4.7 kJ/m$^2$ (more than two-fold increase to the baseline) in the 8PA6-10 + 10 configuration containing nanofibrous layers with a total areal density of 20 g/m$^2$.

## Declaration of competing interest

The authors declare that they have no known competing financial interests or personal relationships that could have appeared to influence the work reported in this paper.

## Data availability

No data was used for the research described in the article.

## Acknowledgements

The research leading to these results has been performed within the framework of the *HyFiSyn* project and has received funding from the European Union's Horizon 2020 research and innovation programme under the *Marie Skłodowska-Curie* grant agreement no. 765881. The research was also supported by the National Research, Development and Innovation Office (NRDI, Hungary) through grant ref. OTKA FK 131882. The research reported in this paper is part of project no. BME-NVA-02, implemented with the support provided by the Ministry of Innovation and Technology of Hungary from the National Research, Development and Innovation Fund, financed under the TKP2021 funding scheme. Gergely Czél is grateful for funding through the Premium Postdoctoral Fellowship Programme and the János Bolyai Research Scholarship of the Hungarian Academy of Sciences. The work was supported by the ÚNKP-22-5-BME-323 New National Excellence Program of the Ministry for Culture and Innovation from the source of the National Research, Development and Innovation Fund. Eva Kuželová Košťáková has received funding from the European Union in the frames of the project "Modular platform for autonomous chassis of specialised electric vehicles for freight and equipment transportation", reg. no. CZ.02.1.01/0.0/0.0/16_025/0007293.

## References

[1] N. Sela, O. Ishai, Interlaminar fracture toughness and toughening of laminated composite materials: a review, Composites 20 (1989) 423–435, https://doi.org/10.1016/0010-4361(89)90211-5.

[2] A. Zucchelli, M.L. Focarete, C. Gualandi, S. Ramakrishna, Electrospun nanofibers for enhancing structural performance of composite materials, Polym. Adv. Technol. 22 (2011) 339–349, https://doi.org/10.1002/pat.1837.

[3] Y Di Boon, S.C. Joshi, A review of methods for improving interlaminar interfaces and fracture toughness of laminated composites, Mater. Today Commun. 22 (2020), 100830, https://doi.org/10.1016/j.mtcomm.2019.100830.

[4] R. Palazzetti, A. Zucchelli, Electrospun nanofibers as reinforcement for composite laminates materials – a review, Compos. Struct. 182 (2017) 711–727, https://doi.org/10.1016/j.compstruct.2017.09.021.

[5] Y. Ou, C. González, J.J. Vilatela, Interlaminar toughening in structural carbon fiber/epoxy composites interleaved with carbon nanotube veils, Compos. Part A Appl. Sci. Manuf. 124 (2019), 105477, https://doi.org/10.1016/j.compositesa.2019.105477.

[6] N.G. Yun, Y.G. Won, S.C. Kim, Toughening of carbon fiber/epoxy composite by inserting polysulfone film to form morphology spectrum, Polymer 45 (2004) 6953–6958, https://doi.org/10.1016/J.POLYMER.2004.08.020.

[7] Y. Swolfs, L. Gorbatikh, I. Verpoest, Fibre hybridisation in polymer composites: a review, Compos. Part A Appl. Sci. Manuf. 67 (2014) 181–200, https://doi.org/10.1016/j.compositesa.2014.08.027.

[8] G. Czél, M.R. Wisnom, Demonstration of pseudo-ductility in high performance glass/epoxy composites by hybridisation with thin-ply carbon prepreg, Compos. Part A Appl. Sci. Manuf. 52 (2013) 23–30, https://doi.org/10.1016/j.compositesa.2013.04.006.

[9] G. Czél, M. Jalalvand, M.R. Wisnom, T. Czigány, Design and characterisation of high performance, pseudo-ductile all-carbon/epoxy unidirectional hybrid composites, Compos. B Eng. 111 (2017) 348–356, https://doi.org/10.1016/j.compositesb.2016.11.049.

[10] S.G. Marino, G. Czél, Improving the performance of pseudo-ductile hybrid composites by film-interleaving, Compos. Part A Appl. Sci. Manuf. 142 (2021), 106233, https://doi.org/10.1016/j.compositesa.2020.106233.

[11] S.G. Marino, F. Mayer, A. Bismarck, G. Czél, Effect of plasma-treatment of interleaved thermoplastic films on delamination in interlayer fibre hybrid composite laminates, Polymers 12 (2020) 2834, https://doi.org/10.3390/polym12122834.

[12] R. Palazzetti, X. Yan, A. Zucchelli, Influence of geometrical features of electrospun nylon 6,6 interleave on the CFRP laminates mechanical properties, Polym. Compos. 35 (2014) 137–150, https://doi.org/10.1002/pc.22643.

[13] K. Molnár, E. Košťáková, L. Mészáros, The effect of needleless electrospun nanofibrous interleaves on mechanical properties of carbon fabrics/epoxy laminates, Express Polym. Lett. 8 (2014) 62–72, https://doi.org/10.3144/expresspolymlett.2014.8.

[14] T. Meireman, L. Daelemans, E. Van Verre, W. Van Paepegem, K. De Clerck, Nanofibre toughening of dissimilar interfaces in composites, Mater. Des. 195 (2020), 109050, https://doi.org/10.1016/j.matdes.2020.109050.

[15] S.V. Lomov, K. Molnár, Compressibility of carbon fabrics with needleless electrospun PAN nanofibrous interleaves, Express Polym. Lett. 10 (2016) 25–35, https://doi.org/10.3144/expresspolymlett.2016.4.

[16] H. Saghafi, T. Brugo, G. Minak, A. Zucchelli, The effect of PVDF nanofibers on mode-I fracture toughness of composite materials, Compos. B Eng. 72 (2015) 213–216, https://doi.org/10.1016/J.COMPOSITESB.2014.12.015.

[17] H. Saghafi, A. Zucchelli, R. Palazzetti, G. Minak, The effect of interleaved composite nanofibrous mats on delamination behavior of polymeric composite materials, Compos. Struct. 109 (2014) 41–47, https://doi.org/10.1016/J.COMPSTRUCT.2013.10.039.

[18] L. Liu, Z.-M. Huang, G.-Y. Xu, Y.-M. Liang, G.-H. Dong, Mode II interlaminar delamination of composite laminates incorporating with polymer ultrathin fibers, Polym. Compos. 29 (2008) 285–292, https://doi.org/10.1002/PC.20367.

[19] L. Liu, Y.M. Liang, G.Y. Xu, H.S. Zhang, Z.M. Huang, Mode I interlaminar fracture of composite laminates incorporating with ultrathin fibrous sheets, J. Reinf. Plast. Comp. 27 (2008) 1147–1162, https://doi.org/10.1177/0731684407086504.

[20] M. Jalalvand, G. Czél, M.R. Wisnom, Damage analysis of pseudo-ductile thin-ply UD hybrid composites - a new analytical method, Compos. Part A Appl. Sci. Manuf. 69 (2015) 83–93, https://doi.org/10.1016/j.compositesa.2014.11.006.

[21] M. Jalalvand, G. Czél, M.R. Wisnom, Parametric study of failure mechanisms and optimal configurations of pseudo-ductile thin-ply UD hybrid composites, Compos. Part A Appl. Sci. Manuf. 74 (2015) 123–131, https://doi.org/10.1016/j.compositesa.2015.04.001.

[22] R. Palazzetti, A. Zucchelli, C. Gualandi, M.L. Focarete, L. Donati, G. Minak, et al., Influence of electrospun Nylon 6,6 nanofibrous mats on the interlaminar properties of Gr-epoxy composite laminates, Compos. Struct. 94 (2012) 571–579, https://doi.org/10.1016/j.compstruct.2011.08.019.

[23] G. Czél, M. Jalalvand, M.R. Wisnom, Hybrid specimens eliminating stress concentrations in tensile and compressive testing of unidirectional composites, Compos. Part A Appl. Sci. Manuf. 91 (2016) 436–447, https://doi.org/10.1016/j.compositesa.2016.07.021.

[24] A. Kelly, W.R.R. Tyson, Tensile properties of fibre-reinforced metals: copper/tungsten and copper/molybdenum, J. Mech. Phys. Solid. 13 (1965) 329–350, https://doi.org/10.1016/0022-5096(65)90035-9.

[25] G. Czél, M. Jalalvand, M.R. Wisnom, Demonstration of pseudo-ductility in unidirectional hybrid composites made of discontinuous carbon/epoxy and continuous glass/epoxy plies, Compos. Part A Appl. Sci. Manuf. 72 (2015) 75–84, https://doi.org/10.1016/j.compositesa.2015.01.019.